Measurements of contrast sensitivity by an adaptive optics visual simulator

Tatsuo Yamaguchi & Keiji Ucikawa

Optical Review

ISSN 1340-6000
Volume 22
Number 4

Opt Rev (2015) 22:629-636
DOI 10.1007/s10043-015-0100-y

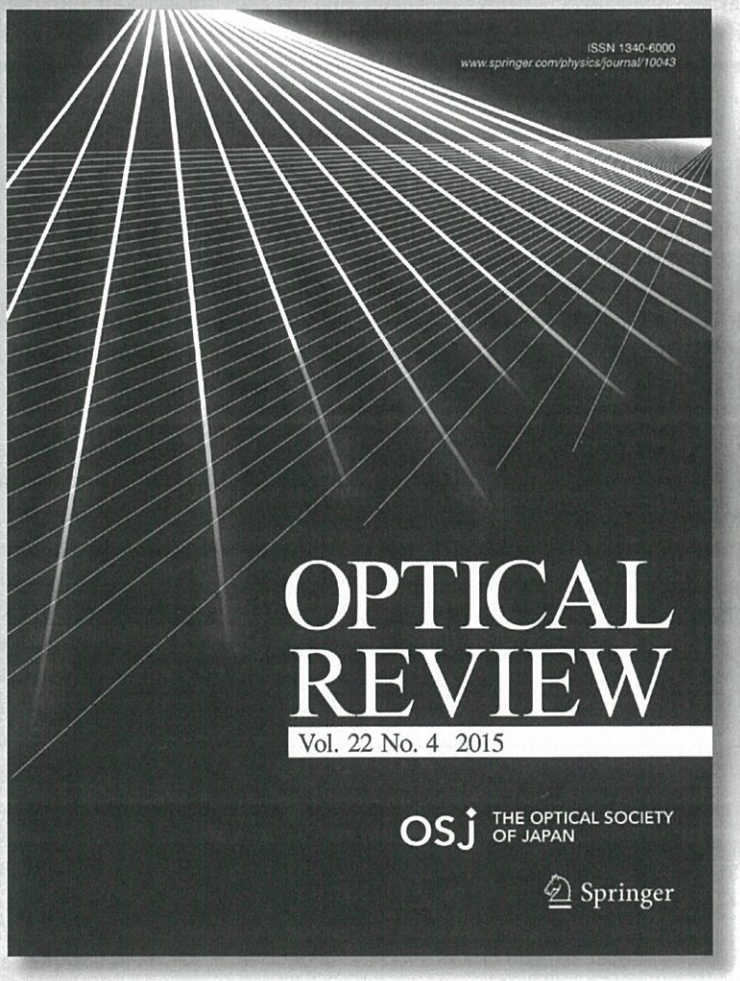

Springer

Opt Rev (2015) 22:629–636
DOI 10.1007/s10043-015-0100-y

REGULAR PAPER

Measurements of contrast sensitivity by an adaptive optics visual simulator

Tatsuo Yamaguchi[1,2] · **Keiji Ucikawa**[1]

Received: 27 January 2015 / Accepted: 17 May 2015 / Published online: 29 May 2015

Abstract We developed an adaptive optics visual simulator (AOVS) to study the relationship between the contrast sensitivity and higher-order wavefront aberrations of human eyes. A desired synthetic aberration was virtually generated on a subject eye by the AOVS, and red laser light was used to measure the aberrations. The contrast sensitivity was measured in a psychophysical experiment using visual stimulus patterns provided by a large-contrast-range imaging system, which included two liquid crystal displays illuminated by red light emitting diodes from the backside. The diameter of the pupil was set to 4 mm by an artificial aperture, and the retinal illuminance of the stimulus image was controlled to 10 Td. Experiments conducted with four normal subjects revealed that their contrast sensitivity to a high-spatial-frequency vertical sinusoidal grating pattern was lower in the presence of a horizontal coma aberration than in the presence of a vertical coma or no aberrations ($p < 0.02$, Nagai method).

Keywords Adaptive optics visual simulator · Contrast sensitivity · Liquid crystal phase modulator

✉ Tatsuo Yamaguchi
t-yamaguchi@topcon.co.jp

[1] Department of Information Processing, Tokyo Institute of Technology, 4259 Nagatsuta-cho, Midori-ku, Yokohama, Kanagawa 226-8503, Japan

[2] Topcon Corporation, 75-1 Hasunuma-cho, Itabashi-ku, Tokyo 174-8580, Japan

1 Introduction

Contrast sensitivity, which is the visual ability to distinguish slight luminance differences, has attracted interest as an important measure of visual performance and visual acuity [1]. Researchers have quantified contrast sensitivity using various techniques, including subjective examinations with a low-contrast sinusoidal stimulus chart with different spatial frequencies or an interference fringe that is directly illuminated on the retina [2–4]. The relationship between contrast sensitivity and myopia was reported by Liou et al. [5]. They suggested that contact lens correction improved contrast sensitivity at high spatial frequencies for subjects with high myopia. However, the effect of the higher-order wavefront aberrations of the eye was not considered in previous studies.

Adaptive optics (AO) technology, which was proposed in the field of astronomy and applied to ophthalmology [6, 7], enables the simulation of arbitrary aberrations of the eyes. To investigate the relationship between wavefront aberrations and visual performance, AO technology has been applied to create an adaptive optics visual simulator (AOVS), which includes a visual stimulus apparatus. Yoon et al. measured visual performance after correcting ocular wavefront aberrations [8]. They used a deformable mirror with 37 actuators. Manzanera et al. studied visual acuity using AO with a liquid crystal light modulator [9], measuring the depth of focus using an AOVS. The effects of Zernike wavefront aberrations on visual acuity have been reported by Rocha et al. [10]. They concluded that custom wavefront correction significantly improved visual acuity compared with best-spectacle correction.

Many of these AOVSs, which are aimed at testing visual acuity, employ a Snellen chart or a Landolt ring chart. These targets are provided by high-contrast displays, such

as conventional cathode ray tubes (CRTs), liquid crystal displays (LCDs), or microdisplays. AOVSs require a device that can display low-contrast images for contrast sensitivity measurements [11]. Although the stimulus image is presented in visible light, AOVSs typically employ infrared light to measure wavefront aberrations [12]. Llorente et al. noted significant differences in higher order aberrations of the human eye between visible light and infrared light [13]. To prevent inaccuracies due to the chromatic aberration of the eyes, wavefront aberrations should be tested with visible light. The measurement of wavefront aberrations with visible light is more accurate when the stimulus image is also visible light. Aberrations with conventional eye glasses can be measured using visible light because the light is not reflected on the glasses, which have an anti-reflection coating.

In this paper, we introduce an AOVS that can simulate arbitrary aberrations, measure aberrations with visible light and display an arbitrary visual stimulus from very low contrast to high contrast. To examine the relationship between the contrast sensitivity and higher-order wavefront aberrations of human eyes at several frequencies, we measured the contrast sensitivity of human eyes in cases in which no aberrations were applied and cases in which higher-order aberrations were intentionally added to the subject's eyes with an AOVS.

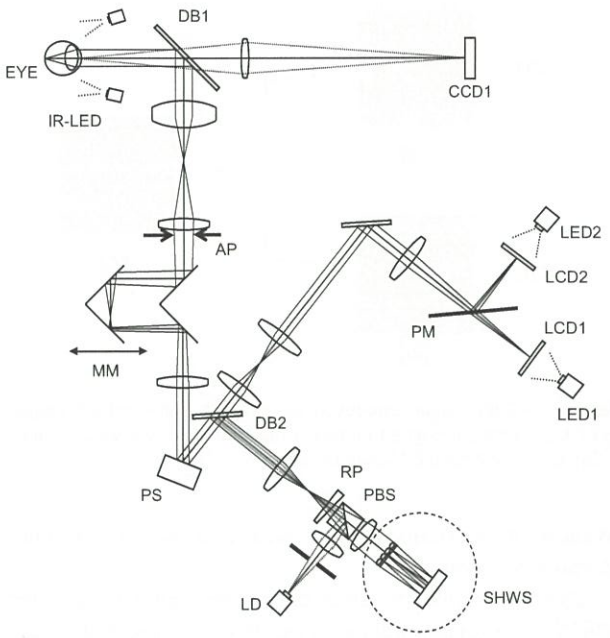

Fig. 1 A schematic of the AOVS. *IR-LED* infrared LED (940 nm), *LD* laser diode, *DB1* dichroic beam splitter to reflect visual stimulus and light from LD and pass 940 nm IR-LED light, *CCD1* CCD to observe the eye position, *AP* artificial aperture, *MM* moving mirror system to correct the spherical error of the subject's eye, *PS* PAL-SLM, *DB2* dichroic beam splitter to reflect LD light and pass visual stimulus light, *RP* rotating prism, *SHWS* Shack–Hartmann wavefront sensor, *PM* pellicle mirror to combine light from LCD1 and LCD2

2 Methods

2.1 Apparatus

The developed AOVS consisted of a liquid crystal phase modulator, wavefront sensor, observation system of the anterior segment, and optical projection system (Fig. 1). The optics of the AOVS had an area of 400 × 450 mm. An artificial aperture (AP in Fig. 1) was inserted into the optical path at the optically conjugate position with respect to the pupil of the subject's eye. Using the artificial aperture, the pupil size was set to 4.0 mm. The retinal illuminance of the stimulus image was controlled to 10 Td. Thus, the subject's pupil was always opened beyond 4.0 mm due to the low light intensity used in this experiment. Cone photoreceptor cells are predominantly responsible for vision at this intensity. The stimulus image was optically located in the far field of the subject's eye by moving the mirror (MM in Fig. 1).

The desired wavefront aberrations were generated by a PAL-SLM reflective liquid crystal phase modulator (X8267-12, Hamamatsu Photonics, Hamamatsu, Japan) at the optically conjugate position with respect to the pupil of the subject's eye. This device can also modulate the phase of the light between 0 and 2π radians. The modulator had a very high resolution of 768 × 768 pixels and a precise linear phase response of 256 levels [14]. The PAL-SLM was controlled by a personal computer in the same manner as conventional VGA devices. These characteristics enabled the AOVS to generate various aberrations.

A Shack–Hartmann wavefront sensor (SHWS) was employed to measure the total aberrations that are inherent to the subject's eye and intentionally generated by the phase modulator. The SHWS consisted of a binary optics lenslet array and a charge coupled device (CCD; C8484, Hamamatsu Photonics, Hamamatsu, Japan). The light source for the wavefront sensing was a 690-nm-wavelength fiber-pigtailed laser diode (LD; FiberMax, Blue Sky Research, Milpitas, CA, USA). The red LD was utilized to measure the wavefront aberrations of the eye to reduce chromatic aberrations. The radiant power at the cornea was 0.5 μW. The duration of the LD was set to 100 ms, which was less than the maximum permissible exposure according to the ANSI standards for the safe use of lasers [15]. The LD was turned off during a contrast sensitivity measurement because the light from the LD disturbed the stimulus images. To reduce speckle and noise from the Shack–Hartmann image, a rotary wedged prism (RP in Fig. 1) was placed in the light path at the optically conjugate position with respect to the pupil of the eye.

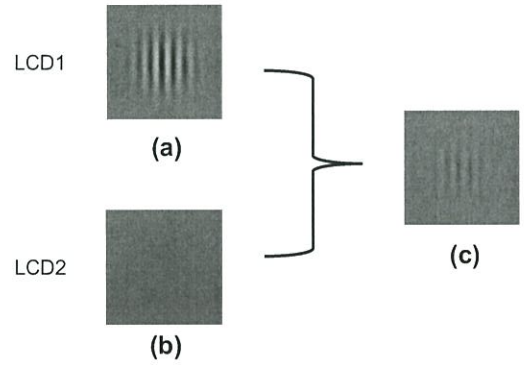

Fig. 2 **a** LCD1 image employed to create a high-contrast image. **b** LCD2 image employed to create a bias image. **c** A visual stimulus created to combine the high-contrast and bias images

Wavefront aberrations were measured up to 6th-order Zernike polynomials.

The observation system of the anterior segment included illuminators and an imager. Two 940-nm-wavelength light emitting diodes (LEDs) illuminated the anterior part of the eye, which was imaged on the CCD (CCD1 in Fig. 1) by the optical system. The center of the pupil was calculated from the obtained image at 30 frames per second. Using the microdrive actuator in the chin rest, the center of the pupil was automatically aligned at the center of the optical system during measurement.

The optical projection system included two conventional 256-level liquid crystal displays (LCD; L3P08X-8x, Seiko Epson, Suwa, Japan), which were located at the optically conjugate position with respect to the retina of the eye. Because both of these LCDs lacked a large contrast range, we illuminated the LCDs from the backside with power-controlled red LEDs and combined the two images provided by the LCDs using a thin pellicle mirror. The stimulation proceeded such that one LCD displayed a grating pattern image of spatially modulated luminance while the other displayed a gray image, as shown in Fig. 2. By independently controlling the light power of the LED retro-illumination for the LCD, we obtained a composited grating image suitable for a desired contrast sensitivity test in the range from 1 to 1000. The size of the combined stimulus image was 1.05 × 1.05 degrees, and the pixel number of the image was 768 × 768.

2.2 Stimuli

Vertical sinusoidal grating pattern images were employed to measure contrast sensitivity. The spatial frequency of the grating image is five (2.3, 3.9, 6.5, 10.8 and 18 cycles per degree). After the contrast thresholds at each frequency were measured, the results were plotted as the subject's contrast sensitivity function. Seven stimulus contrast steps were employed for each frequency. The minimum contrast sensitivity was determined in advance by the method of adjustment.

The contrast threshold was determined in sequential two-alternative forced choice tasks. Figure 3 shows the generation of the stimulus images. When no stimulus was present, a frame was displayed on the outer portion of the screen to ensure that the direction of the subject's eye remained fixed on the image area. The color of the frame resembled that of the stimulus images. The retinal illuminance of the frame was 10 Td. The stimulus images were presented in the following order: (1) the frame; (2) a grating image or the gray image for 0.3 s with a beep sound; (3) the frame for 0.5 s; (4) the gray image or a grating image for 0.3 s with a beep sound; and (5) the frame. In step (2), either the grating image or the gray image was presented in a random order, and the image presented in step (4) was different from that presented in step (2). The subject identified the grating image using a joypad. The contrast of the next grating image was two steps greater in the case of an incorrect answer and one step lower for correct answers. This experiment was conducted 120 times over two days (60 times per day) at each spatial frequency.

To measure the contrast threshold, we fit the data points of 1/contrast versus probability correct to a psychometric function using a maximum likelihood criterion [16]. We defined the contrast threshold as a 0.75 probability of being correct for the psychometric function. An example of the psychometric function is shown in Fig. 4.

2.3 Procedure

The experiment was conducted in a dark room to completely dilate the subject's pupil. The spherical and cylindrical errors of the eye were measured by a clinical wavefront aberrometer prior to the experiment. The subject wore glasses with a cylindrical trial lens to reduce their cylindrical aberration. A cylindrical trial lens was

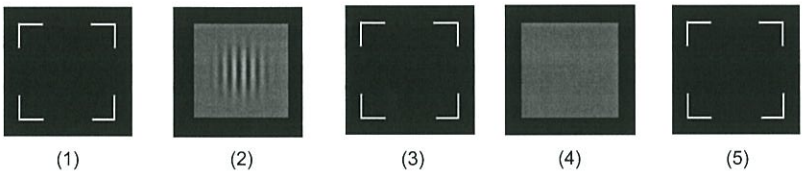

Fig. 3 Generation of stimulus images. **1** Frame, **2** grating pattern image (or gray image), **3** frame, **4** Gray image (or grating pattern image), **5** frame

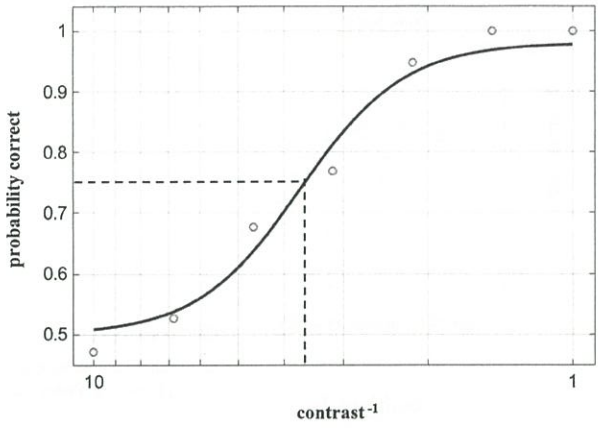

Fig. 4 Example of psychometric function fitting

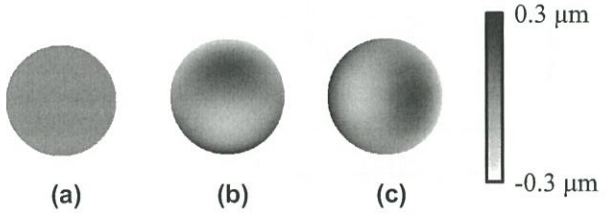

Fig. 5 Wavefront aberration configurations. **a** Compensating aberrations of the eye. **b** Adding vertical coma aberration (RMS 0.1 μm) after compensating eye aberrations. **c** Adding horizontal coma aberration (RMS 0.1 μm) after compensating eye aberrations. The diameter of each pupil is 4 mm

employed due to the limited capacity of the PAL-SLM to correct aberrations. The spherical errors were corrected by moving component MM in the apparatus. The subject's head and chin were set on a chin rest, and the subject observed the stimulus images. The wavefront aberrations of the eye were measured by turning on the LD prior to the experiment. The MM component was moved in small steps based on the measured aberration to optically position the subject's focus at the subject's far point.

We conducted an experiment to determine the contrast threshold without compensating for higher order aberrations, where the adaptive optics system was not employed and lower order aberrations were compensated with the trial lens and the MM component. Subsequently, the adaptive optics system was used to apply the following three wavefront configurations: (a) compensating for aberrations of the eye (no aberrations), where the root mean square (RMS) of the residual aberrations was less than 0.01 μm; (b) adding a vertical coma as a Zernike coefficient C_3^{-1} to obtain an RMS of 0.1 μm after compensating for aberrations; and (c) adding a horizontal coma as a Zernike coefficient C_3^1 to obtain an RMS of 0.1 μm after compensating for aberrations (Fig. 5). The three wavefront configurations (a), (b) and (c) were defined as

Table 1 Subjects' demographic data and manifest refraction

Subject	Age (Y)	Sex	Sph (D)	Cyl (D)	Axis (deg)
1	35	M	−5.0	−2.1	4
2	38	M	−7.6	−1.0	143
3	40	F	−8.5	−1.0	14
4	45	F	−3.9	−0.3	177

NA, VCA and HCA, respectively. The wavefront aberrations were measured to confirm the total aberration. After the aberration was made suitable for the simulation of the wavefront configuration, the contrast sensitivity measurements were begun. Experiments were conducted in each wavefront configuration.

2.4 Subjects

We utilized the right eyes of four subjects. All subjects had normal healthy eyes and wore glasses for far vision in their daily lives. Table 1 shows the subjects' demographics and optical characteristics.

3 Results

The contrast sensitivity functions for four subjects with NA and without compensating for higher-order aberrations are shown in Fig. 6. The horizontal axis shows the spatial frequency, and the vertical axis shows the contrast sensitivity. The error bars represent the standard error of the mean. The smooth curves are the best double exponential fits to the data [17]. The p values were calculated using the Nagai method [18]. The p values at 10.8 and 18 cycles per degree (c/deg) for subject 4 were less than 0.01. The other p values were greater than 0.3. Figure 7 shows the wavefront maps of each subject's eye and the corresponding RMS without compensating for higher-order aberrations.

Figure 8 shows the contrast sensitivity functions of four subjects with NA, VCA and HCA. Table 2 presents the statistical significance (p values) of the differences between NA and VCA and between NA and HCA at 18 c/deg. At this frequency, all four subjects exhibited a decrease in the contrast sensitivity with HCA compared with other aberrations ($p < 0.02$). Note that the contrast threshold could not be obtained with HCA for subjects 2 and 3. When we compared NA with VCA at 18 c/deg, a decrease in the contrast sensitivity was found for all subjects in VCA. However, the decrease was not larger in HCA for subjects 1 and 4. The contrast threshold was obtained in VCA for subjects 2 and 3. We calculated the RMS errors of the difference between NA and VCA (DNV) and between NA and HCA (DNH) with the sum of the four subjects' contrast

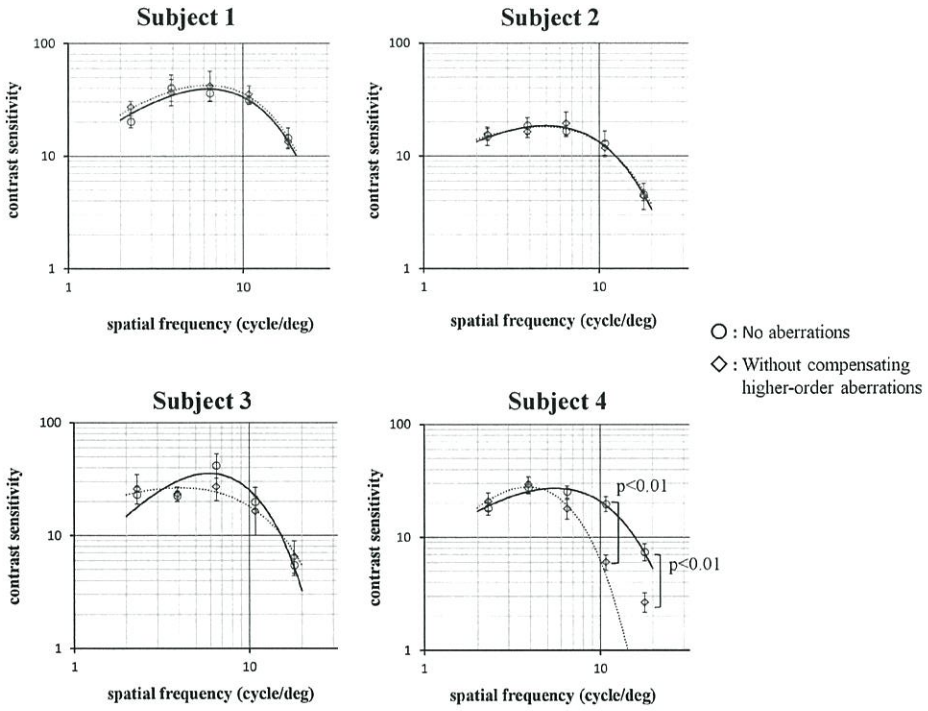

Fig. 6 Contrast sensitivity functions for four subjects with no aberrations and without compensating higher order aberrations

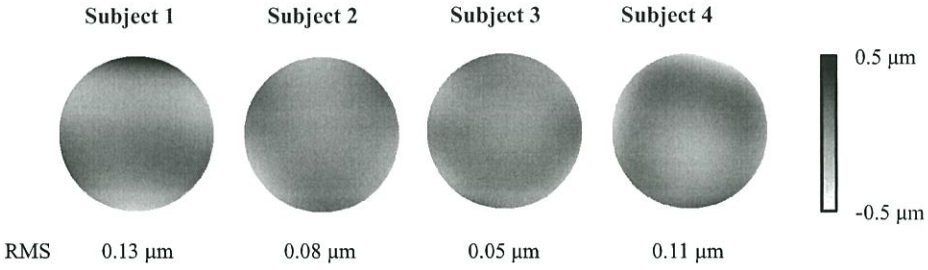

Fig. 7 Wavefront maps and RMS for four subjects without compensating higher order aberrations

thresholds, excluding DNH at 18 c/deg for subjects 2 and 3 because the contrast threshold could not be obtained with HCA. The RMS values of DNV and DNH were 0.057 ± 0.008 (in log units) and 0.087 ± 0.002, respectively, at lower frequencies (2.3 and 3.9 c/deg) and 0.203 ± 0.008 and 0.325 ± 0.007, respectively, at higher frequencies (10.8 and 18 c/deg). The differences in the contrast sensitivity at higher frequencies were greater than those at lower frequencies.

4 Discussion

In this study, we confirmed the value of using AOVS, in which a red laser light was used to measure aberrations and stimulate large-contrast-range images. The contrast sensitivity function can be measured in several wavefront configurations using the AOVS in a psychophysical experiment. The results of our experiment show that the contrast sensitivity function was affected by the type of wavefront aberration. Figure 6 compares functions with NA and functions without compensating for higher-order aberrations. Although no significant difference in the contrast sensitivity was observed for three of the subjects, significant differences at higher frequencies (10.8 and 18 c/deg) were observed for subject 4 ($p < 0.01$). This result suggests that the higher-order wavefront aberrations of human eyes may have different effects on contrast sensitivity for different individuals, especially at higher frequencies.

The results indicate that the contrast sensitivity was significantly lower with HCA. To test the effect of wavefront configurations, we examined the point spread functions and simulated the high-contrast grating image at 18 c/deg with NA, VCA and HCA (Fig. 9). We calculated the ratios determined by the minimum and maximum values in

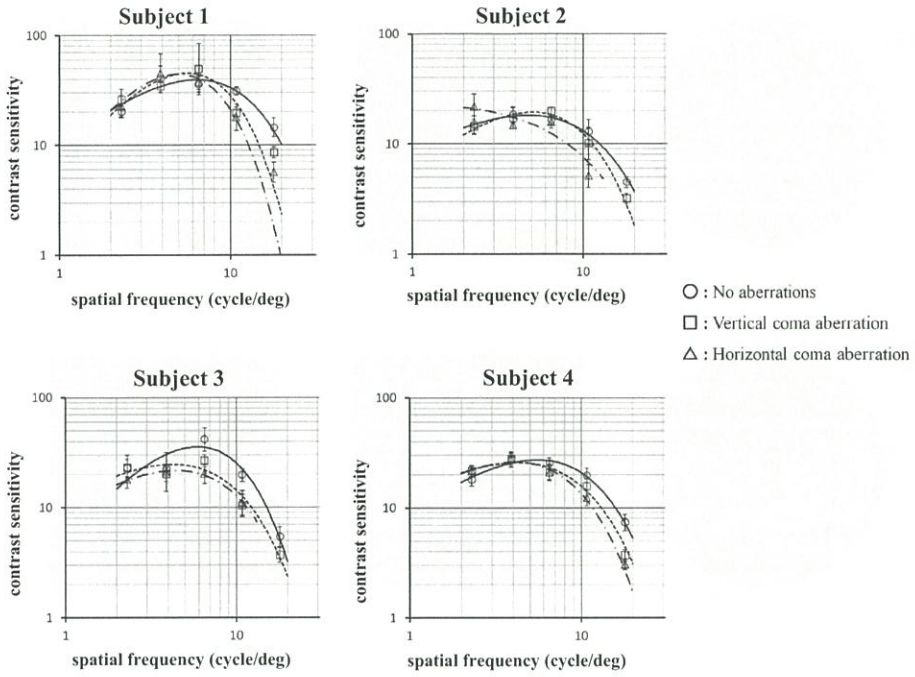

Fig. 8 Contrast sensitivity functions for four subjects with no aberration, vertical coma aberration and horizontal coma aberration

Table 2 Statistical significance (p values, Nagai method) of the differences between no aberration and vertical or horizontal coma aberration at 18 c/deg

Spatial frequency	Subject 1		Subject 2		Subject 3		Subject 4	
	NA and VCA	NA and HCA	NA and VCA	NA and HCA	NA and VCA	NA and HCA	NA and VCA	NA and HCA
18	$p < 0.02$	$p < 0.01$	$p < 0.01$	ND	$p < 0.02$	ND	$p < 0.01$	$p < 0.01$

NA and *VCA* No aberrations and vertical coma aberration

NA and *HCA* No aberrations and horizontal coma aberration

ND No data were collected because a constant threshold could not be obtained

the simulated images of VCA and HCA. The ratios for VCA and HCA were approximately 4 and 1.5, respectively. We found that HCA degraded the vertical grating image to a greater extent than VCA. These simulations suggest that the decrease in the contrast sensitivity may be attributed to the type of wavefront aberration and the grating image.

Figure 10 shows the optical modulation transfer functions (MTFs) for the various wavefront configurations along the horizontal direction in the simulation. These MTFs were calculated using a 4.0-mm-diameter pupil. Evidently, the MTFs were degraded for both HCA and VCA compared with NA at high spatial frequencies. Artal et al. previously described the association between the MTF and the contrast sensitivity [19], reporting that the contrast sensitivity decreased at higher frequencies than the MTF. However, it seems that the curve of the contrast sensitivity function of subject 2 with NA did not significantly differ from that with VCA but did significantly differ from that with MTF. We calculated the RMS errors of the curves of the contrast sensitivity function between NA and VCA to confirm the difference between the curves. The RMS error for subject 2 was 0.07 in log units, the lowest value obtained for any of the subjects (subject 1: 0.16, subject 3: 0.27, subject 4: 0.10). All subjects in this experiment had myopia and wore glasses in their daily lives; thus, we measured the wavefront aberrations of the four subjects while they wore their glasses. The RMS values of the Zernike coefficients C_3^{-1} were as follows: subject 1, 0.15 μm; subject 2, 0.29 μm; subject 3, 0.01 μm; and subject 4, 0.18 μm. Subject 2 had the highest RMS of the four subjects and a larger vertical coma aberration in daily life. This visual experience may cause the correction of the blurred image. This hypothesis is thought to be related to Yoon's report [20], which suggests

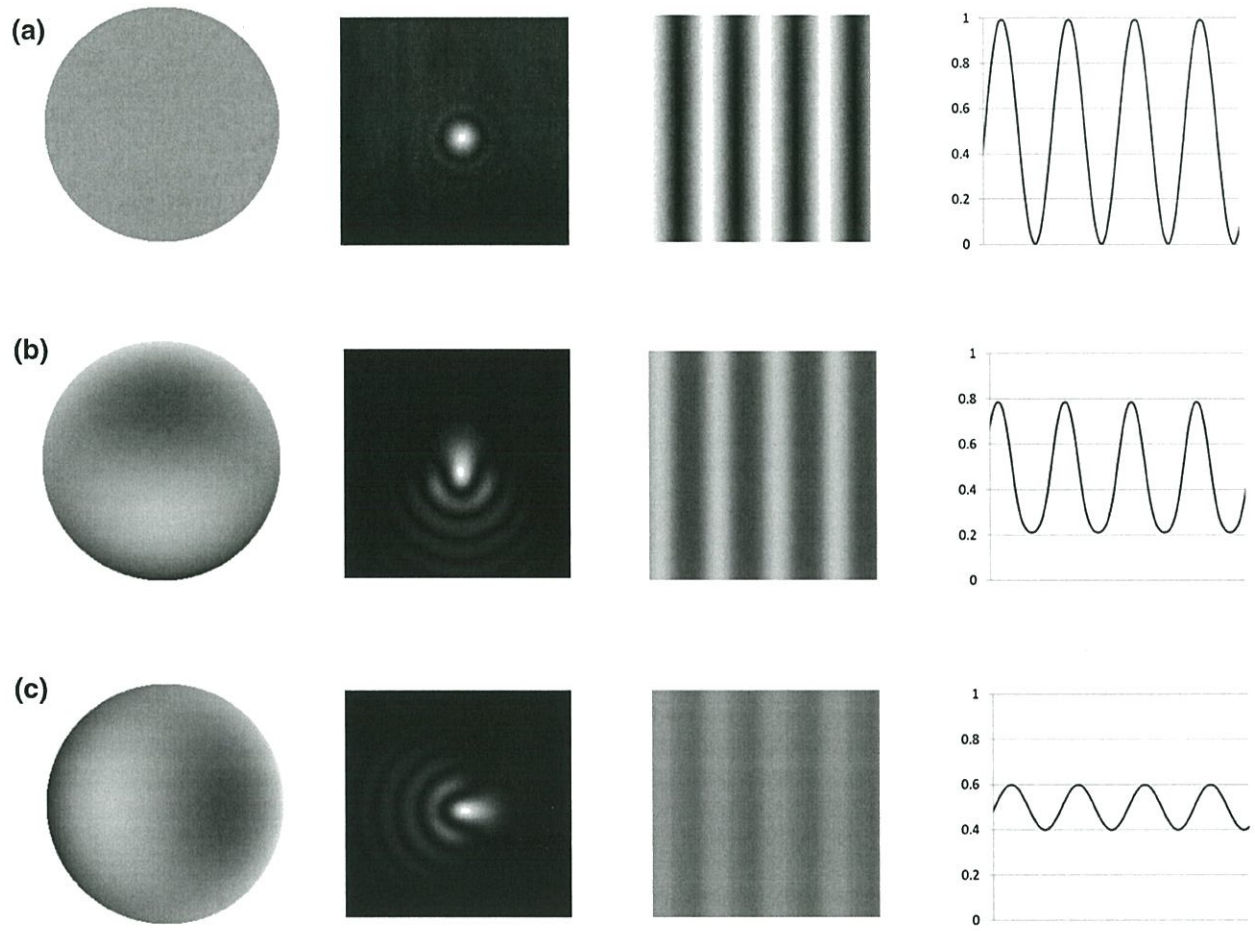

Fig. 9 Wavefront aberrations, point spread functions, simulations of high-contrast grating image and graphs of horizontal cross sections of the simulations at 18 c/deg. **a** No aberration, **b** vertical coma aberration, **c** horizontal coma aberration

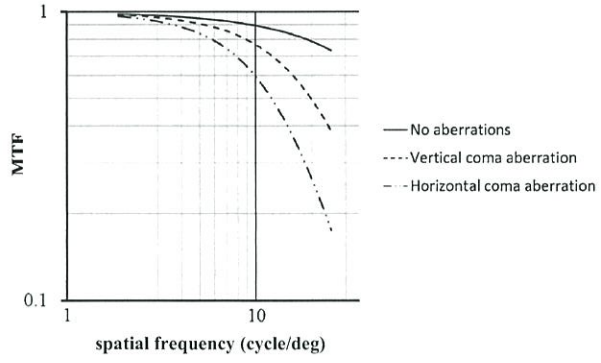

Fig. 10 MTF plots of simulations in three wavefront configurations about the horizontal direction

that long-term visual experience with poor retinal image quality may restrict the visual benefit achieved immediately after correction. In the future, we hope to conduct experiments using a horizontal sinusoidal grating pattern with VCA and HCA to explore the effect of the long-term visual experience caused by aberrations.

We developed an AOVS with two LCDs for use with glasses to measure the contrast sensitivity function while preventing chromatic aberration. These characteristics make this tool useful for psychophysical experiments measuring contrast sensitivity. The AOVS is also a powerful aid for glasses and contact lens design and refractive surgery, with the potential to improve the outcomes of these processes in the future.

Acknowledgments This research was supported by Topcon Corporation, Japan. The authors appreciate Professor Toshifumi Mihashi's helpful advice and thank Dr. Yoko Hirohara, Mr. Joji Ichimura and Ms. Akemi Miwa for their cooperation in collecting data.

References

1. Barten, P.G.J.: Contrast Sensitivity of the Human Eye and its Effects on Image Quality, p. 25. SPIE Press, Washington (1999)
2. Nes, F.L., Bouman, M.A.: Spatial modulation transfer in the human eye. J. Opt. Soc. Am. **57**, 401 (1967)

3. Peli, E., Arend, L.E., Young, G.M., Goldstein, R.B.: Contrast sensitivity to patch stimuli: effects of spatial bandwidth and temporal presentation. Spat. Vis. **7**, 1 (1993)
4. Coletta, N.J., Sharma, V.: Effects of luminance and spatial noise on interferometric contrast sensitivity. J. Opt. Soc. Am. A: **12**, 2244 (1995)
5. Liou, S.W., Chiu, C.J.: Myopia and contrast sensitivity function. Curr. Eye Res. **22**, 81 (2001)
6. Roddier, F.: Adaptive Optics in Astronomy, p. 3. Cambridge University Press, New York (1999)
7. Liang, J., Williams, D.R., Miller, D.T.: Supernormal vision and high-resolution retinal imaging through adaptive optics. J. Opt. Soc. Am. A: **14**, 2884 (1997)
8. Yoon, G.Y., Williams, D.R.: Visual performance after correcting the monochromatic and chromatic aberrations of the eye. J. Opt. Soc. Am. A: **19**, 266 (2002)
9. Manzanera, S., Prieto, P.M., Ayala, D.B., Lindacher, J.M., Artal, P.: Liquid crystal adaptive optics visual simulator: application to testing and design of ophthalmic optical elements. Opt. Express **15**, 16177 (2007)
10. Rocha, K.M., Vabre, L., Harms, F., Chateau, N., Krueger, R.R.: Effects of Zernike wavefront aberrations on visual acuity measured using electromagnetic adaptive optics technology. J. Refract. Surg. **23**, 953 (2007)
11. Agostini, T., Bruno, N.: Lightness contrast in CRT and paper-and-illuminant displays. Percept. Psychophys. **58**, 250 (1996)
12. Prieto, P., Fernandez, E., Manzanera, S., Artal, P.: Adaptive optics with a programmable phase modulator: applications in the human eye. Opt. Express **12**, 4059 (2004)
13. Llorente, L., Santana, L.D., Saucedo, D.L., Marcos, S.: Aberrations of the human eye in visible and near infrared illumination. Optom. Vis. Sci. **80**, 26 (2003)
14. Fukuchi, N., Biqing, Y., Igasaki, Y., Yoshida, N., Kobayashi, Y., Hara, T.: Oblique-incidence characteristics of a parallel-aligned nematic-liquid-crystal spatial light modulator. Opt. Rev. **12**, 372 (2005)
15. American National Standard for Safe Use of Lasers, p. 15. Laser Institute of America, Florida (2007)
16. Prins, N., Frederick, K.: Psychophysics: A Practical Introduction, p. 69. Academic Press, Utah (2010)
17. Movshon, J.A., Kiorpes, L.: Analysis of the development of spatial contrast sensitivity in monkey and human infants. J. Opt. Soc. Am. A: **5**, 2166 (1988)
18. Nagai, T., Hoshino, T., Uchikawa, K.: Statistical significance testing of thresholds estimated by constant stimuli method. See. Perceiving **24**, 91 (2011)
19. Artal, P., Marcos, S., Iglesias, I., Green, D.G.: Optical modulation transfer and contrast sensitivity with decentered small pupils in the human eye. Vis. Res. **36**, 3575 (1996)
20. Sabesan, R., Yoon, G.: Visual performance after correcting higher order aberrations in keratoconic eyes. J. Vis. **96**, 1 (2009)